ACS APPLIED MATERIALS & INTERFACES

Research Article

Cite This: ACS Appl. Mater. Interfaces 2018, 10, 2937−2945

www.acsami.org

Spatiotemporal Characteristics of Intercellular Calcium Wave Communication in Micropatterned Assemblies of Single Cells

Fulin Xing,[†] Ping Zhang,[†] Pengchong Jiang,[†] Ziyuan Chen,[†] Jianyu Yang,[†] Fen Hu,[†] Irena Drevenšek-Olenik,[‡] Xinzheng Zhang,[†] Leiting Pan,*[,†,§] and Jingjun Xu*[,†,∥]

[†]The Key Laboratory of Weak-Light Nonlinear Photonics of Education Ministry, School of Physics and TEDA Applied Physics Institute, and [§]The 2011 Project Collaborative Innovation Center for Biological Therapy, Nankai University, Tianjin 300071, China

[‡]Faculty of Mathematics and Physics, University of Ljubljana, and J. Stefan Institute, Ljubljana SI1000, Slovenia

[∥]Collaborative Innovation Center of Extreme Optics, Shanxi University, Taiyuan, Shanxi 030006, China

Supporting Information

ABSTRACT: Micropatterned substrates offer a unique possibility to define and control spatial organization of biological cells at the microscale, which greatly facilitates investigations of the cell-to-cell communication in vitro. Here, we developed a simple micropatterning strategy to resolve various spatiotemporal characteristics of intercellular calcium wave (ICW) communication among isolated BV-2 microglial cells. By using a single-ring assembly, we found that the direction of the initial transmitter secretion was strongly correlated with the site of the cell at which the mechanical stimulus triggering the ICWs was imposed. By using multiring assemblies, we observed that the response ratio of the same outmost cells 160 μm away from the center increased from 0% in the single-ring assembly to 9.6% in the four-ring assembly. This revealed that cells located in the interring acted as regenerative amplifiers for the ICWs generated by the central cell. By using a special oval-type micropattern, we found that calcium mobilization in lamellipodia of a fusiform BV-2 microglia cell occurred 2.9 times faster than that in the middle part of the cell, demonstrating a higher region-specific sensitivity of lamellipodia to the transmitter. Taken together, our micropatterning strategy opened up new experimental prospects to study ICWs and revealed novel spatiotemporal characteristics of ICW communication including stimulation site-dependent secretion, regenerative propagation, and region-specific cell sensitivity.

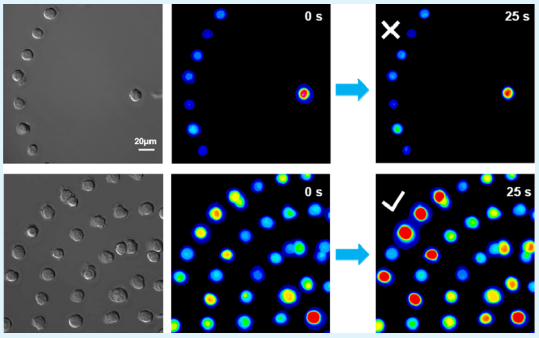

KEYWORDS: *micropatterning, intercellular calcium waves, paracrine pathway, regenerative propagation, microglial cells*

1. INTRODUCTION

Cells of multicellular organisms need to communicate with each other to share information and facilitate various functions.[1,2] One of the principal forms of cell-to-cell communication is intercellular calcium waves (ICWs). They regulate numerous biological activities including vascular tone regulation,[3,4] developmental modulation,[5] electrical activity modification,[6,7] hepatic glucose mobilization,[8] synaptic connectivity organization,[9] and immune activation.[10,11] Propagation of ICWs between physically connected cells takes place via gap junctions,[12,13] whereas the paracrine pathway mediates the ICW propagation between physically isolated cells. In the paracrine pathway, signaling molecules (transmitter) secreted by an individual cell diffuse across the extracellular medium and are subsequently sensed by the neighboring cells that respond with calcium mobilization.[14] Despite a considerable progress in understanding the characteristics of ICWs made during the last decades, many important details, such as the spatial range of the transmitter or different mechanisms of signal regeneration and amplification, still lack a satisfactory level of understanding because effective spatially and temporally resolved experimental approaches are missing.

Micropatterning techniques, such as photolithography, soft lithography, and microcontact printing, have recently revealed broad application prospects in biomedical research including biosensing,[15,16] genetic analysis,[17] tissue engineering,[18,19] cell-based drug testing,[20,21] and low-cost diagnostics and high-throughput screening.[22,23] They also enabled an important opportunity to study fundamental characteristics of cellular morphology,[24,25] cell migration,[26,27] and proliferation and differentiation at the single-cell level.[28,29] As they provide precise control of spatial locations of the cells, they are also very suitable for the investigation of intercellular communication processes, in particular those mediated by ICWs. For instance, by using micropatterning to connect bone cells into linear cell chains, hexagonal cell loops, and 2D cell networks,[30,31] it was recently found that paracrine, rather than gap junctions, is

Received: October 16, 2017
Accepted: December 28, 2017
Published: December 28, 2017

DOI: 10.1021/acsami.7b15759
ACS Appl. Mater. Interfaces 2018, 10, 2937−2945

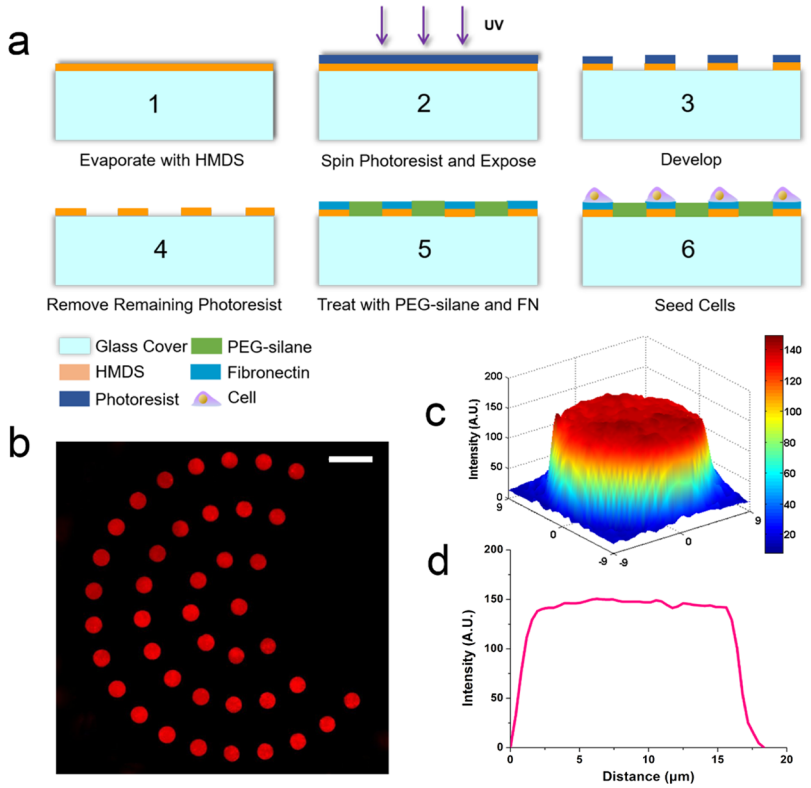

Figure 1. Schematic drawing of the preparation of patterned substrates and the distribution of the Cy3.5FN dye on these substrates. (a) Fabrication procedure. Glass substrates coated with HMDS are spun-cast with a photoresist and exposed to designed patterns. FN is connected to HMDS-covered islands and nonHMDS-covered area is passivated with PEG−silane. (b) Fluorescence image of Cy3.5FN bound to HMDS-covered islands. Scale bar = 50 μm. (c) 3D projection of the Cy3.5 fluorescence intensity of the central island in (b). (d) Cross section of the intensity profile shown in (c).

dominantly involved in ICWs elicited by mechanical stimuli. Micropatterning also facilitated determination of the propagation velocity of ICWs and of their maximum range within multicellular clusters of varying sizes.[32,33]

In this study, we developed a simple micropatterning strategy to organize BV-2 microglial cells into spatially discrete patterns composed of single cells. BV-2 microglial cells belong to an immortalized mouse microglial cell line that is known to largely exemplify functional features of primary microglia.[34−37] Such a patterning requires a combination of a subtle pattern design with gentle cell manipulation and single-cell detection. A set of ring-type assemblies and an oval-type micropattern were designed to study the ICW communication induced by localized microstimulation. Our observations revealed several novel spatiotemporal characteristics of the ICWs associated with transmitter secretion, its propagation, and its sensitivity by neighboring cells.

2. MATERIALS AND METHODS

2.1. Cell Culture. The BV-2 microglial cells were cultured in Dulbecco's modified Eagle's medium (Gibco, USA) containing 10% (v/v) fetal bovine serum (Biological Industries, USA), 100 U/mL penicillin, and 100 μg/mL streptomycin (Gibco, USA) at 37 °C in a humidified incubator at 5% CO_2. Before being planted on substrates, the cells were detached from the culture flasks with 0.25% trypsin + 0.04% EDTA (Gibco, USA) and diluted to the density of 8×10^5 mL^{-1}.

2.2. Substrate Preparation. Glass substrates were cleaned by immersion into a chromic acid lotion and then baked at 80 °C for 20 min. Afterward, they were placed for 21 min into a hermetic flask containing hexamethyldisilazane (HMDS, Sigma, USA) to enable vapor phase deposition. A positive photoresist (RuiHong, China) was spun-cast on the HMDS-treated substrates. Then, the photoresist was exposed to UV light through a chrome-based photomask. The exposed photoresist was removed by a developing solution. Subsequently, the substrates were treated with 2 min oxygen plasma treatment to remove the exposed HMDS. The remaining photoresist was dissolved with acetone and rinsed with isopropanol and deionized (DI) water to uncover the underlying HMDS micropattern. Afterward, the substrates were submerged for 20 h into 3 mM poly(ethylene glycol) (PEG)−silane (Gelest, USA) solution in anhydrous toluene containing 1% (v/v) of triethylamine (Sigma, USA) to achieve stable passivation. Then, they were sonicated for 5 min in anhydrous toluene, ethanol, and DI water, successively, to remove the physically adsorbed PEG−silane. At the end, they were dried with nitrogen. Fibronectin (FN, Sigma, USA) was dissolved in phosphate-buffered saline (PBS) to a concentration of 150 μg/mL and spread at 4 °C for 15 min onto the prepared substrates. After the FN solution was removed, cell suspension was planted on the substrates at 37 °C for 20 min. The suspended cells were washed away, and the remaining cells were located on the designed patterns. The resulting patterned cell assemblies were used for experiments within 1 h after preparation.

To label the FN with fluorescence, the FN solution was mixed with a reactive dye (Cy3.5, GE Healthcare, UK) for 20 min, and then it was spread onto the substrates prepared. Cy3.5FN was excited by a mercury lamp using a 546/12 nm excitation filter, and fluorescence emission was collected by a fluoro 40×/1.30 oil objective combined with a 590/35 nm emission filter.

2.3. Ca^{2+} Imaging. The imaging of cytosolic calcium concentration ($[Ca^{2+}]_c$) was performed as described previously.[38] BV-2 microglial cells were loaded with 2 μM calcium-sensitive Fluo-4 AM (Invitrogen, USA) for 30 min at 37 °C in Hanks balanced salt solution (HBSS, 140 mM NaCl, 5 mM KCl, 2 mM $CaCl_2$, 1 mM $MgCl_2 \cdot 6H_2O$, 10 mM glucose, 10 mM HEPES, pH 7.4). Then, they were washed

DOI: 10.1021/acsami.7b15759
ACS Appl. Mater. Interfaces 2018, 10, 2937−2945

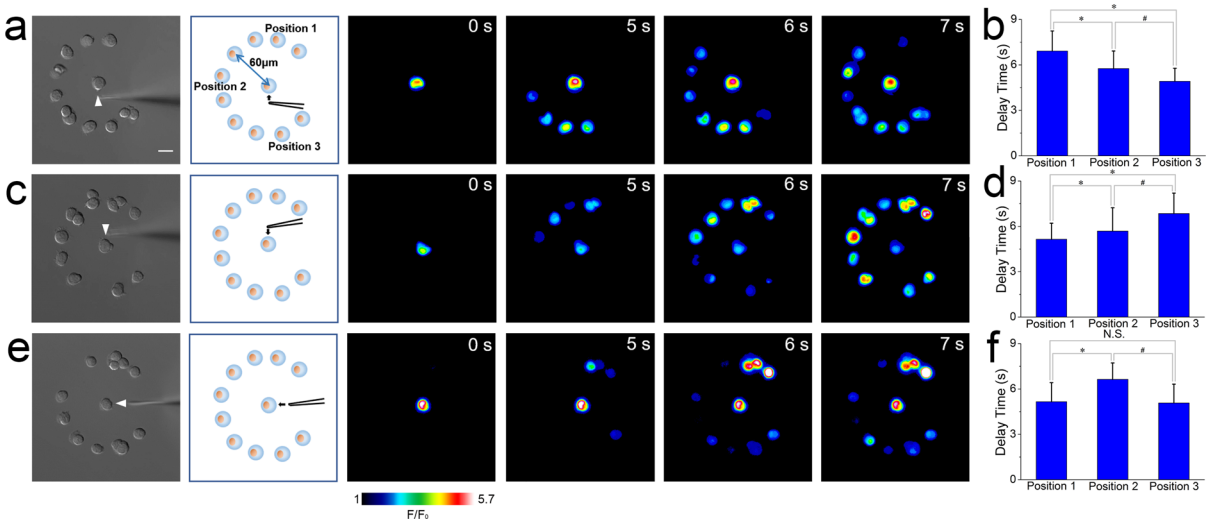

Figure 2. ICWs arrive first at the outer cells nearest to the stimulation site at the central cell. Sequences of pseudocolor images show the mechanical stimulation-elicited propagation of ICWs among BV-2 microglial cells assembled in a single-ring concentric pattern with a radius of 60 μm. White arrowheads indicate the application site of the mechanical stimulus. (a) Glass microelectrode approaches the central cell from below, and thus, the lower site of the central cell is stimulated. The ICWs exhibit a clockwise propagation. Scale bar = 20 μm. (b) Delay times of the cells in positions 1, 2, and 3 for (a) (n = 10). *P < 0.05, compared to position 1 group; #P < 0.05, compared to position 2 group. (c) Upper site of the central cell is stimulated, and the ICWs show an anticlockwise propagation. (d) Delay times of the cells in positions 1, 2, and 3 for (c) (n = 10). *P < 0.05, compared to position 1 group; #P < 0.05, compared to position 2 group. (e) Right site of the central cell is stimulated, and the ICWs propagate synchronously from both ends of the ring. (f) Delay times of the cells in positions 1, 2, and 3 for (e) (n = 10). N.S., no significant difference. *P < 0.05, compared to position 1 group; #P < 0.05, compared to position 2 group.

with HBSS for 10 min for de-esterification of the intracellular AM esters. The Fluo-4-loaded cells were excited by a mercury lamp using a 485/20 nm excitation filter, and fluorescence emission was collected by a fluoro 40×/1.30 oil objective combined with a 540/50 nm emission filter. Sequences of images were captured by an electron multiplying charge-coupled device (DU-897D-CS0-BV, Andor, U.K.) mounted on the inverted fluorescent microscope (Axio Observer D1, Carl Zeiss, Germany). Two different arrangements were used: (a) pulsed exposure with a duration of 50 ms and a repetition rate of 1 Hz followed by subsequent image capturing and (b) continuous exposure combined with continuous image capturing at a rate of ∼20 frames/s. Modifications of fluorescence intensities within the selected regions of interest were analyzed by MetaMorph software (Universal Imaging Corp., USA). A relative fluorescence intensity F/F_0, defined as the intensity detected after stimulation divided by the basal intensity before stimulation, was chosen to depict the spatiotemporal characteristics of the $[Ca^{2+}]_c$ level in the selected cell.

2.4. Mechanical Stimulus. It has been established that the application of mechanical stimulus was an extensively used method in the study of intercellular Ca^{2+} signaling.[5,7,33,39] In the present work, individual cells were stimulated by a glass microelectrode (1 μm tip diameter) that was mounted on a three-axis micromanipulator (MMO-202ND, Narishige, Japan) attached to an inverted fluorescent microscope (Axio Observer D1, Carl Zeiss, Germany). The tip of the microelectrode was moved toward the selected cell and used to provoke a gentle mechanical stimulus on its surface. Before applying the mechanical stimulus to the central cell, all cells were in a resting state with a stable basal $[Ca^{2+}]_c$ (F/F_0 = 1).

2.5. Propidium Iodide Staining. The propidium iodide powder (Beyotime, China) was dissolved in PBS to the concentration of 10 μg/mL. Cells were loaded with propidium iodide solution for 5 min at room temperature. Then, propidium iodide solution was removed, and cells were washed three times with PBS. Propidium iodide was excited with a 546/12 nm excitation filter, and fluorescence emission was collected with a 590/35 nm emission filter.

2.6. Statistical Analysis. A particular cell was regarded as responsive to the transmitter when it presented a rise of $[Ca^{2+}]_c$, resulting in $(F_{max}/F_0) > 1.1$. The responsivity of a particular group of the cells was calculated as the ratio between the number of responding cells and the total number of cells in the group. The delay time of the response was calculated as the time interval between the calcium rise in the central cell and the peripheral cells. The obtained data were presented as mean ± SD. A statistical comparison between two groups was analyzed using Student's t-test implemented by the IBM software SPSS (version 22). Results with P < 0.05 were considered to be statistically significant.

3. RESULTS AND DISCUSSION

3.1. Secretion of the Transmitter from the Stimulated Site of the Cell. One of the challenges of pattern designing was to determine the proper size of adhesive islands to bond only single cells. Cells might not firmly adhere to islands that are much smaller than the cells. On the contrary, big islands might attract more than one cell, thus reducing the accuracy of the patterning. To find the optimal size, we assessed average sizes of circular and fusiform BV-2 microglial cells deposited on standard nonpatterned substrates. According to the diameter observed for the circular cells, which was 16.6 ± 1.7 μm (Figure S1), we decided to use a photomask with circular apertures of 18 μm in diameter. To test the spatial distribution of the extracellular matrix (FN) on the patterned substrates, the premixed Cy3.5FN solution was spread on the substrates prepared as shown in Figure 1a. The resulting fluorescence distribution is shown in Figure 1b–d, which revealed that FN almost homogeneously covered the area of the predetermined HMDS islands within the diameter of 16 μm, thus providing appropriate sites for cell adhesion.

The first aim of our investigation was to allocate the secreting site of the transmitter that mediated the generation of ICWs by the stimulated cell. In this purpose, BV-2 microglial cells were planted on the concentric pattern containing a single ring with a diameter of 60 μm. Mechanical stimulus was applied from three different directions: from below, from above, and from the right as shown in the scheme of Figure 2a,c,e. In all cases, it triggered a rapid rise of $[Ca^{2+}]_c$ in the central cell that was

DOI: 10.1021/acsami.7b15759
ACS Appl. Mater. Interfaces 2018, 10, 2937–2945

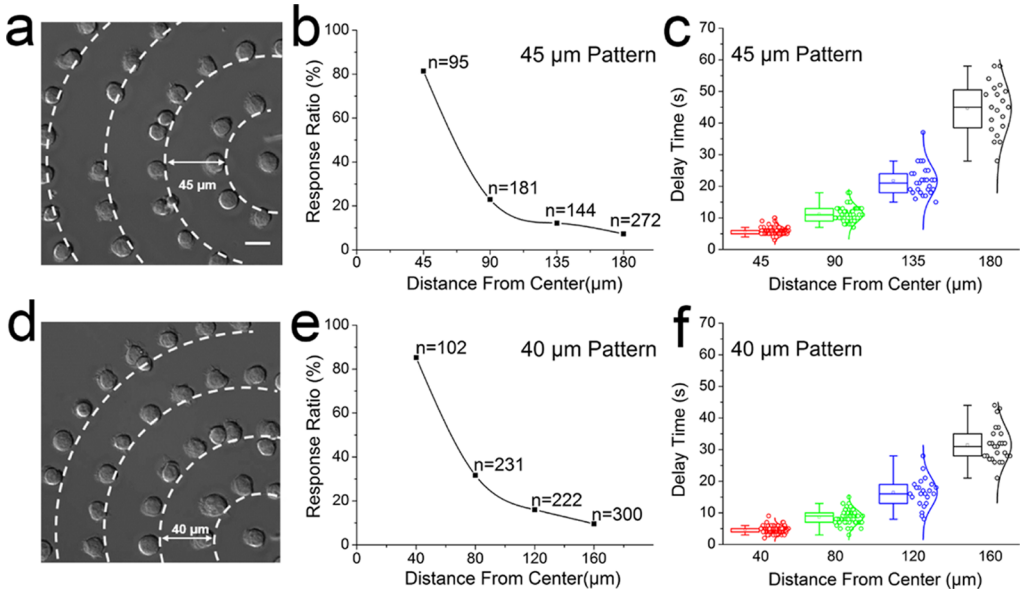

Figure 3. Response ratio of the outer cells decreases and the delay time of their response increases with increasing distance from the central cell. (a) Representative image of BV-2 microglia cells planted on the 45 μm distance pattern visualized by differential interference contrast. The dashed lines indicate the single ring of cells. Scale bar = 20 μm. (b) Response ratio of the cells decreases as the distance from the central cell increases in the 45 μm distance pattern. *n* is the total number of measured cells in the group. (c) Statistical data for the observed delay times of cellular responses detected in the 45 μm distance pattern. The average delay time of the cells located in the specific ring increases with increasing distance of the ring from the central cell. (d) Cells planted on the 40 μm distance pattern. (e) Response ratio of the cells in the 40 μm distance pattern. The responsivity decreases with increasing distance from the central cell. (f) Statistical delay times of cellular responses detected in the 40 μm distance pattern. The delay time increases with increasing distance of the ring from the central cell.

followed by propagation of the ICWs to the outer cells, which responded with some time delay. In addition, the integrity of the plasma membrane was monitored all time to ensure that no visible permanent membrane deformation or cellular detachment took place after the mechanical stimulus. An appropriate stimulus, as used in our ICW studies, caused recoverable deformation on the plasma membrane (Supporting Information, Movie 1), while excessive mechanical stress resulted in membrane blebbing followed by the uptake of propidium iodide, which indicated membrane damage and cell death (Figure S2).

By analyzing video-microscopy images, we found that calcium responses of the outer cells were not simultaneous, but, as can be seen in Figure 2, the ICWs were at first detected by the cells located opposite to the stimulated site of the central cell. We selected three positions (labeled as positions 1, 2, and 3 in Figure 2) in the ring and calculated the average delay times of cellular response in these positions. A clockwise propagation manner was observed when the central cell was stimulated from below (Figure 2a, Supporting Information, Movie 2). The corresponding delay times were 4.9 ± 0.9, 5.8 ± 1.2, and 6.9 ± 1.3 s for positions 3, 2, and 1, respectively (Figure 2b). An anticlockwise propagation manner was observed when the central cell was stimulated from above (Figure 2c, Supporting Information, Movie 3) with delay times of 5.2 ± 1.0, 5.7 ± 1.5, and 6.9 ± 1.4 s for positions 1, 2, and 3, respectively (Figure 2d). When the stimulus was imposed from the right side, a symmetric propagation occurred (Figure 2e, Supporting Information, Movie 4) with delay times of 5.2 ± 1.3, 6.6 ± 1.1, and 5.1 ± 1.2 s for positions 1, 2, and 3, respectively (Figure 2f). Therefore, the ICWs at first approached the cells nearest to the stimulus site of the central cell. From these observations, we concluded that the transmitter secretion was site-dependent, that is, the transmitter mediating the ICWs was secreted from the stimulated site of the cell.

Some previous work demonstrated that the extracellular adenosine triphosphate (ATP) acted as the ICW transmitter in glial cells.[39−41] A high dose of ligands will desensitize the receptors, so they cannot be activated by the following stimulation.[38] Thus, to confirm the secretion of ATP from the stimulated cell, we applied 1 μM ATP to desensitize corresponding ATP receptors involved in the propagation of ICWs. The results showed that the added ATP significantly inhibited mechanical stimulation-elicited ICWs (Figure S3, Supporting Information, Movie 5), which proved that the secretion of ATP occurred from the stimulated cell. In addition, the exact secreting site on the mechanical stimulated cell was not resolved in previous work. On the basis of micropatterning, our study revealed that the transmitter was secreted from the stimulated site of the cell, which was probably associated with local activation of hemichannels,[42] ion channels, and vesicular discharge on the plasma membrane induced by its mechanical deformation.[43,44] The site-dependent generation of the transmitter provides an interesting possibility to control the propagation direction of the ICWs.

3.2. ICWs in the Patterned Cell Assembly Propagating in a Distance-Dependent Manner. To quantitatively investigate the propagation of ICWs between single BV-2 microglial cells assembled in the patterned configuration, 2 four-ring concentric patterns with different distances between the rings were designed, namely, 45 μm (45 μm distance pattern) and 40 μm (40 μm distance pattern) (Figure 3a,d, Supporting Information, Movies 6 and 7). The outmost rings were 180 and 160 μm away from the center. The cells were planted on the substrates, and their Ca^{2+} activity was monitored after stimulation of the central cell. It was found that the level of calcium response decreased with increasing distance from

DOI: 10.1021/acsami.7b15759
ACS Appl. Mater. Interfaces 2018, 10, 2937−2945

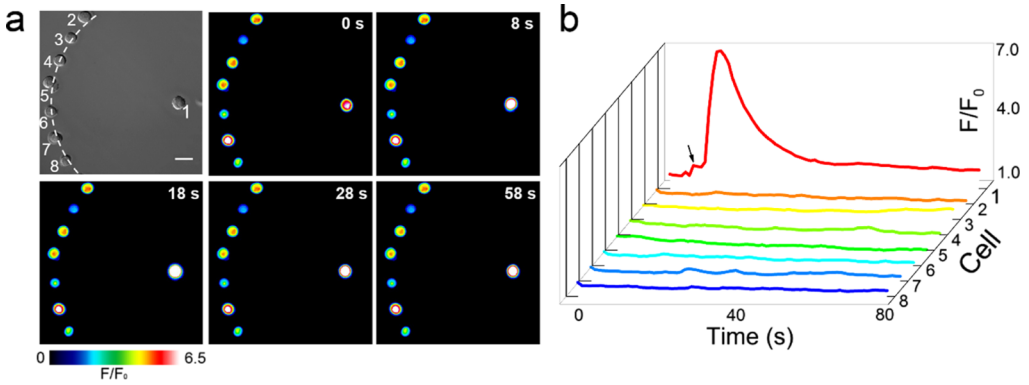

Figure 4. ICWs generated by the central cell are not sensed by the cells located in the ring that are 160 μm away from the center. (a) Time sequence of pseudocolor images of $[Ca^{2+}]_c$ in BV-2 microglial cells planted on the single-ring concentric pattern with a radius of 160 μm. The dotted line indicates the single ring of cells. Scale bar = 20 μm. (b) $[Ca^{2+}]_c$ traces of the single cells denoted as cell nos. 1−8 in (a). The arrow indicates the application of mechanical stimulus on the cell no. 1. None of the cells in the ring are responsive.

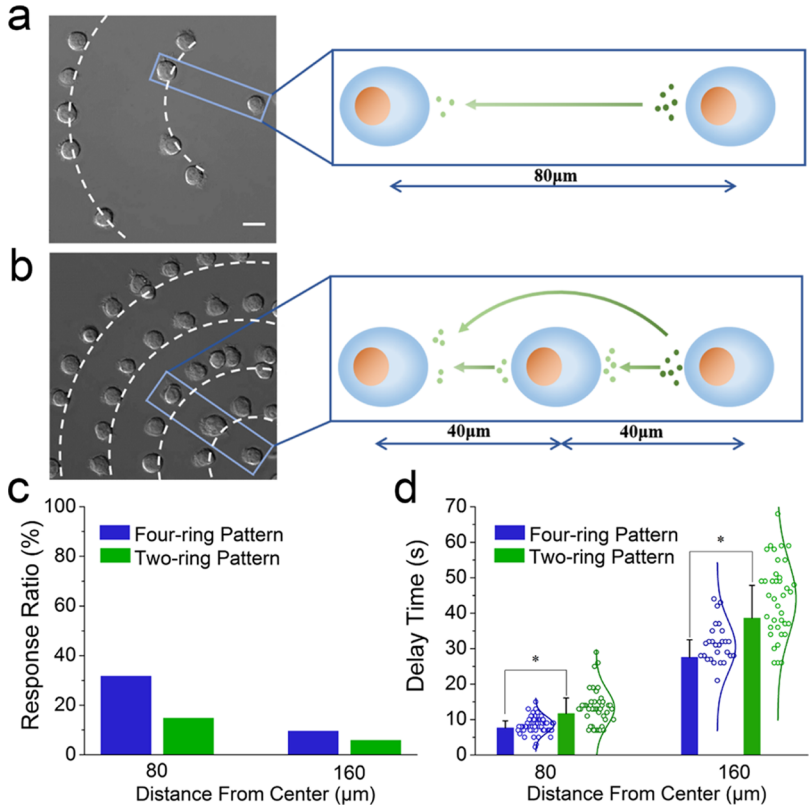

Figure 5. Presence of relay station cells increases the responsivity and reduces the response delay of the outer cells. (a) Cells in the two-ring concentric pattern. The transmitter secreted from the central cell diffuses to cells in the ring 80 μm from the center. The dashed lines indicate the cells in the same ring. Scale bar = 20 μm. (b) Cells in the four-ring concentric pattern. The transmitter secreted from the central cell and relay station cells in the ring 40 μm from the center diffuses to the cells in the ring that are 80 μm away from the center. (c) Response ratios of cells in the rings that are 80 and 160 μm away from the center in the two-ring and four-ring patterns. The response ratio of the cells in the two-ring pattern is lower than that in the four-ring pattern. (d) Response delay of the cells in the rings that are 80 and 160 μm away from the center in the two-ring and in the four-ring patterns (the number of measured cells $n \geq 181$ in both configurations). *$P < 0.05$.

the center. Specifically, in the 45 μm distance pattern, calcium response ratios were 81.4, 22.9, 12.2, and 7.3% for the cells located at distances L = 45, 90, 135, and 180 μm from the central cell, respectively (Figure 3b). In the 40 μm distance pattern, calcium response ratios were 85.3, 31.7, 16.0, and 9.6% for distances L = 40, 80, 120, and 160 μm, respectively (Figure 3e). The delay time of the response increased with increasing distance. In the 45 μm distance pattern, the observed delay times were τ_d = 5.8 ± 1.3, 11.2 ± 2.4, 21.7 ± 4.7, and 44.7 ± 8.2 s for the cells located at distances L = 45, 90, 135, and 180 μm from the central cell, respectively (Figure 3c). In the 40 μm distance pattern, the observed delay times were τ_d = 4.2 ± 1.1, 8.7 ± 2.2, 16.4 ± 4.4, and 31.5 ± 5.6 s for distances L = 40, 80, 120, and 160 μm, respectively (Figure 3f). The corresponding dependencies of $\tau_d(L)$ were fitted to the power law $\tau_d \propto L^S$. The values of S were 2.1 ± 0.3 with a coefficient of determination R^2 = 0.98 for the 45 μm distance pattern (Figure S4a) and 1.9 ± 0.2 with R^2 = 0.97 for the 40 μm

DOI: 10.1021/acsami.7b15759
ACS Appl. Mater. Interfaces 2018, 10, 2937−2945

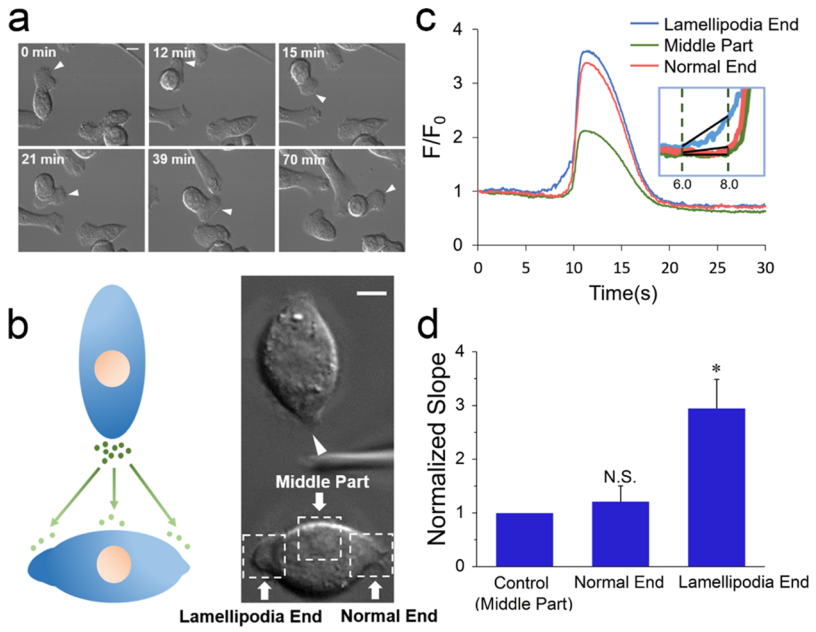

Figure 6. Lamellipodia end exhibits faster calcium mobilization than other regions of the cell. (a) Lamellipodia as the leading edge of a migrating BV-2 microglial cell. The white arrowhead indicates the lamellipodia. Scale bar = 10 μm. (b) BV-2 microglial cells planted on oval patterns. Lamellipodia is located at the left end of the lower cell. The white arrow indicates the site of mechanical stimulus. Scale bar = 10 μm. (c) Calcium traces in three regions of the lower cell after stimulus was applied to the upper cell. Mobilization of $[Ca^{2+}]_c$ in the lamellipodia end is faster than that in the other two regions. The inset illustrates determination of the slopes between the starting point of calcium mobilization and the point 2 s behind the starting point for the three traces. (d) Relative slopes with respect to the middle part (n = 35 for lower cells). All values are expressed as mean ± SD. N.S., no significant difference. *P < 0.05.

distance pattern (Figure S4b). This indicated the diffusive nature of the propagation of ICWs.

3.3. Intermediate Cells Acting as Regenerative Amplifiers ("Relay Stations") of the Transmitter. ATP-induced extra ATP release was observed in astrocytes through the detection of radioactive-labeled ATP.[45] This result provided the probability of the regenerative mechanism. In addition, Hassinger's study implied possible existence of the regenerative releasing of the transmitter that mediated the ICWs.[46] Some theoretical studies presented mathematical models considering a point source ATP release in combination with its partial regeneration to depict the regenerative mechanism.[47,48] Thus, to examine the role of neighboring cells on the propagation of ICWs, we designed concentric ring patterns with different numbers of rings.

At first, we used a single-ring pattern with a diameter of 160 μm. We observed that, after stimulation of the central cell, the cells located 160 μm away from the center did not show any calcium response (Figure 4a,b, Supporting Information, Movie 8). This suggested that the range of ICWs in the extracellular medium was below 160 μm. However, if the four-ring pattern with 40 μm interring distance was used, as mentioned before, the response ratio of the same outmost cells 160 μm away from the center was 9.6% (Figure 3c). This signified that the cells positioned on the intermediate rings acted as "relay stations" that released some additional transmitter into the extracellular medium and consequently enabled propagation of ICWs to the outer ring. This result revealed that spatial extension of the ICWs was promoted by the regenerative action of the nearby cells.

To investigate in detail the influence of relay stations on the delay time and the responsivity of the outer cells, we utilized a two-ring concentric pattern with the rings 80 and 160 μm away from the center, respectively (Figure 5a). In comparison with the four-ring pattern with 40 μm interring distance (Figure 5b), the two-ring pattern lacked the innermost ring and the third ring acted as relay station rings. Both the two-ring and the four-ring patterns contained the rings that were 80 and 160 μm away from the center, so we measured the responsivities and delay times of $[Ca^{2+}]_c$ responses in these two rings. We observed that, although they were positioned at the same distance from the center, the cells assembled in the two-ring pattern exhibited lower response ratios and longer delay times (Supporting Information, Movie 9) than analogous cells assembled in the four-ring pattern (Supporting Information, Movie 7). For the cells in the ring that are 80 μm away from the center, the obtained ratios were 31.7% for the four-ring pattern and 16.7% for the two-ring pattern (Figure 5c). The higher response ratio in the four-ring pattern was attributed to the contribution of the transmitter from the relay station cells in the ring that are 40 μm away from the center (Figure 5b). For the cells in the ring that are 160 μm away from the center, the observed ratios were 9.6% (in the four-ring pattern) and 5.8% (in the two-ring pattern) (Figure 5c). Similar differences were also observed for the delay times of the $[Ca^{2+}]_c$ response. The delay time associated with the specific ring was significantly shorter for cells assembled in the four-ring pattern in comparison with those assembled in the two-ring pattern. For the cells in the ring that are 80 μm away from the center, the corresponding delay times were 8.7 ± 2.2 s (in the four-ring pattern) and 13.3 ± 5.0 s (in the two-ring pattern), whereas for the cells in the ring that are 160 μm away from the center, the corresponding values were 31.5 ± 5.6 s (in the four-ring pattern) and 44.1 ± 10.5 s (in the two-ring pattern) (Figure 5d).

Taken together, our observations suggested that in addition to the transmitter released from the stimulated central cell,

DOI: 10.1021/acsami.7b15759
ACS Appl. Mater. Interfaces 2018, 10, 2937–2945

during the propagation of ICWs some extra transmitter was emitted from the relay station cells in the intermediate rings. This caused the associated ICWs to reach the outermost ring faster than in the case without the intermediate rings. Hence, our results directly provided the first experimental evidence of a regenerative amplification process, which were associated with the so-called relay station cells acting as regenerative amplifiers that provided larger propagation speed and wider propagation range of the ICWs.

3.4. Lamellipodia Having Higher Sensitivity for ICWs Than Other Regions of the Cell. In our initial experiment, we observed that BV-2 microglial cells planted on conventional glass substrates exhibited two different cellular morphologies, that is, a circular shape and a fusiform shape. The migrating cells had well-developed lamellipodia in the direction of motion (Figure 6a, Supporting Information, Movie 10). Previous work showed that lamellipodia intended to extend from the blunt end in a teardrop-like pattern and the sharp corners in a square-shaped pattern.[49,50] To verify our conjecture that lamellipodia, as the leading edge of cellular migration,[51] might be more sensitive to an extracellular transmitter than other regions of the cell, we designed oval-shaped adhesive islands with a long axis of 26 μm and a short axis of 18 μm. The cells were planted on them and induced to form lamellipodia at one end of the island (Figure 6b).

To detect differences in the sensitivity to the transmitter molecules between the lamellipodia and other regions of the cell, we created two mutually perpendicular oval patterns to minimize the difference in distances between the secreting site of the upper cell and the three regions of the lower cell, namely, the lamellipodia end, the middle part, and the normal end (Figure 6b). Temporal changes in $[Ca^{2+}]_c$ in the three regions were recorded by acquiring subsequent fluorescence images at the rate of ~20 frames/s. The lower end of the upper cell was stimulated. The analysis of the initial rise of the $[Ca^{2+}]_c$ revealed that the lamellipodia end exhibited the most rapid calcium mobilization, whereas the normal end and the middle part responded almost synchronously (Figure 6c, Supporting Information, Movie 11). To obtain a quantitative measure for the observed effect, we calculated the slope between the starting point of the calcium mobilization and another point 2 s after the starting point (see the inset of Figure 6c). The rising part of the $[Ca^{2+}]_c$ traces is more meaningful than other parts because faster calcium mobilization indicates higher sensitivity to the transmitter. Thus, we compared the rates of calcium mobilization through calculating the slope between the starting point of the calcium mobilization and another point 2 s after the starting point. The corresponding slopes normalized with respect to the slope for the middle part are given in Figure 6d. The slope for the lamellipodia end was 2.9 $\pm$ 0.5 times the slope for the middle part. The slope for the normal end was 1.2 $\pm$ 0.3 times the slope for the middle part (Figure 6d). This result demonstrated that, although the distance between the lamellipodia end and the secreting site was larger than the distance between the middle part and the secreting site, the lamellipodia end reacted more rapidly with calcium mobilization than the middle part, which indicated its higher sensitivity to the transmitter molecules.

This region-specific cell sensitivity might be associated with the distribution of transmitter-sensitive receptors such as nucleotide-sensitive P2Y receptors. Further investigations are needed to clarify the relationship between the distribution of the receptors on the lamellipodia and local differences in the transmitter sensing. Local Ca^{2+} signal has been reported to participate in cell motility and guide cell migration. For instance, it has been demonstrated that the Ca^{2+} level in the uropod of human neutrophils was higher than that in the cell body, which was involved in the regulation of cell locomotion.[52] Besides this, local Ca^{2+} pulses were found to promote lamellipodia retraction and adhesion cycles along the leading edge of moving human umbilical vein endothelial cells.[53,54] Furthermore, calcium flickers assembled in lamellipodia and played a crucial role in steering the migration of fibroblasts.[55,56] A rapid calcium mobilization might provide a feedback mechanism in the regulation of lamellipodia formation. Our observation of the faster calcium mobilization in the lamellipodia might indicate its important role in guiding the cell migration.

4. CONCLUSIONS

In summary, we developed a simple and effective micropatterning strategy by which several novel spatiotemporal characteristics of the ICWs were resolved, including stimulation site-dependent secretion, regenerative propagation, and region-specific cell sensitivity. The stimulation site-dependent feature of transmitter secretion was elucidated through the propagation manner of the ICWs in the single-ring concentric cellular assembly. Furthermore, it was observed that the response ratio of the same outmost cells that are 160 μm away from the center increased from 0% in the single-ring assembly to 9.6% in the four-ring assembly, indicating that ICWs propagated further on account of the regenerative transmitter release from the relay station cells. In addition, an oval-shaped design enabled to resolve that lamellipodia had calcium mobilization 2.9 times faster than the middle part of the cell, showing enhanced sensitivity to the transmitter. We believe that our micropatterning strategy paves a way toward specifically designed experimental investigations on cellular assemblies and consequently toward improved understanding of ICW-based cell–cell communications.

■ ASSOCIATED CONTENT

Supporting Information

The Supporting Information is available free of charge on the ACS Publications website at DOI: 10.1021/acsami.7b15759.

Assessment for average sizes of BV-2 microglial cells on standard nonpatterned substrates; propidium iodide staining for BV-2 microglial cells after mechanical stimulus; ATP desensitization assay of patterned BV-2 microglial cells; and fitting curves of response ratios in 40 and 45 μm patterns (PDF)

Deformation of the mechanically stimulated cell (AVI)

Mechanical stimulation-induced ICW propagation in a clockwise propagation manner (AVI)

Mechanical stimulation-induced ICW propagation in an anticlockwise manner (AVI)

Mechanical stimulation-elicited ICW propagation in a symmetric manner (AVI)

Inhibition of mechanical stimulation-elicited ICWs (AVI)

Mechanical stimulation-elicited ICW propagation in the 45 μm distance four-ring pattern (AVI)

Mechanical stimulation-induced ICW propagation in the 40 μm distance four-ring pattern (AVI)

Mechanical stimulation-elicited ICW propagation in the 160 μm distance single-ring pattern (AVI)

DOI: 10.1021/acsami.7b15759
ACS Appl. Mater. Interfaces 2018, 10, 2937–2945

Mechanical stimulation-induced ICW propagation in the 80 μm distance two-ring pattern (AVI)
Migrating cells with well-developed lamellipodia in the direction of motion (AVI)
Faster calcium mobilization at the lamellipodia end of the cell than other regions of the cell (AVI)

AUTHOR INFORMATION

Corresponding Authors

*E-mail: plt@nankai.edu.cn (L.P.).
*E-mail: jjxu@nankai.edu.cn (J.X.).

ORCID

Leiting Pan: 0000-0001-5329-6114

Author Contributions

L.P. and J.X. conceived the study; F.X., P.J, Z.C., and J.Y. performed the experiments; F.X., P.Z., J.Y., and F.H. analyzed the data; X.Z., L.P., and J.X. provided experimental tools and materials; L.P., F.X., and I.D.-O. wrote the paper; and L.P. and J.X. approved the final paper.

Notes

The authors declare no competing financial interest.

ACKNOWLEDGMENTS

This work was supported by the National Natural Science Foundation of China (no. 11574165), the PCSIRT (no. IRT_13R29), the 111 Project (no. B07013), and the project of bilateral cooperation between Slovenia and China (no. BI-CN/17-18-018).

REFERENCES

(1) Mittelbrunn, M.; Sánchez-Madrid, F. Intercellular Communication: Diverse Structures for Exchange of Genetic Information. *Nat. Rev. Mol. Cell Biol.* **2012**, *13*, 328−335.
(2) Bassler, B. L. Small Talk: Cell-to-cell Communication in Bacteria. *Cell* **2002**, *109*, 421−424.
(3) Attwell, D.; Buchan, A. M.; Charpak, S.; Lauritzen, M.; MacVicar, B. A.; Newman, E. A. Glial and Neuronal Control of Brain Blood Flow. *Nature* **2010**, *468*, 232−243.
(4) Mulligan, S. J.; MacVicar, B. A. Calcium Transients in Astrocyte Endfeet Cause Cerebrovascular Constrictions. *Nature* **2004**, *431*, 195−199.
(5) Weissman, T. A.; Riquelme, P. A.; Ivic, L.; Flint, A. C.; Kriegstein, A. R. Calcium Waves Propagate through Radial Glial Cells and Modulate Proliferation in the Developing Neocortex. *Neuron* **2004**, *43*, 647−661.
(6) Kuga, N.; Sasaki, T.; Takahara, Y.; Matsuki, N.; Ikegaya, Y. Large-scale Calcium Waves Traveling through Astrocytic Networks in Vivo. *J. Neurosci.* **2011**, *31*, 2607−2614.
(7) Newman, E. A.; Zahs, K. R. Calcium Waves in Retinal Glial Cells. *Science* **1997**, *275*, 844−847.
(8) Stümpel, F.; Ott, T.; Willecke, K.; Jungermann, K. Connexin 32 Gap Junctions Enhance Stimulation of Glucose Output by Glucagon and Noradrenaline in Mouse Liver. *Hepatology* **1998**, *28*, 1616−1620.
(9) Katz, L. C.; Shatz, C. J. Synaptic Activity and the Construction of Cortical Circuits. *Science* **1996**, *274*, 1133−1138.
(10) Sieger, D.; Moritz, C.; Ziegenhals, T.; Prykhozhij, S.; Peri, F. Long-range Ca^{2+} Waves Transmit Brain-damage Signals to Microglia. *Dev. Cell* **2012**, *22*, 1138−1148.
(11) Westphalen, K.; Gusarova, G. A.; Islam, M. N.; Subramanian, M.; Cohen, T. S.; Prince, A. S.; Bhattacharya, J. Sessile Alveolar Macrophages Communicate with Alveolar Epithelium to Modulate Immunity. *Nature* **2014**, *506*, 503−506.
(12) Jørgensen, N. R.; Teilmann, S. C.; Henriksen, Z.; Civitelli, R.; Sørensen, O. H.; Steinberg, T. H. Activation of L-type Calcium Channels is Required for Gap Junction-mediated Intercellular Calcium Signaling in Osteoblastic Cells. *J. Biol. Chem.* **2003**, *278*, 4082−4086.
(13) Suadicani, S. O.; Flores, C. E.; Urban-Maldonado, M.; Beelitz, M.; Scemes, E. Gap Junction Channels Coordinate the Propagation of Intercellular Ca^{2+} Signals Generated by P2Y Receptor Activation. *Glia* **2004**, *48*, 217−229.
(14) Leybaert, L.; Sanderson, M. J. Intercellular Ca^{2+} Waves: Mechanisms and Function. *Physiol. Rev.* **2012**, *92*, 1359−1392.
(15) Orth, R. N.; Clark, T. G.; Craighead, H. G. Avidin-biotin Micropatterning Methods for Biosensor Applications. *Biomed. Microdevices* **2003**, *5*, 29−34.
(16) Xing, F.; Meng, G.-X.; Zhang, Q.; Pan, L.-T.; Wang, P.; Liu, Z.-B.; Jiang, W.-S.; Chen, Y.; Tian, J.-G. Ultrasensitive Flow Sensing of a Single Cell Using Graphene-based Optical Sensors. *Nano Lett.* **2014**, *14*, 3563−3569.
(17) Waters, L. C.; Jacobson, S. C.; Kroutchinina, N.; Khandurina, J.; Foote, R. S.; Ramsey, J. M. Multiple Sample PCR Amplification and Electrophoretic Analysis on a Microchip. *Anal. Chem.* **1998**, *70*, 5172−5176.
(18) Ho, C.-T.; Lin, R.-Z.; Chen, R.-J.; Chin, C.-K.; Gong, S.-E.; Chang, H.-Y.; Peng, H.-L.; Hsu, L.; Yew, T.-R.; Chang, S.-F.; Liu, C.-H. Liver-cell Patterning Lab Chip: Mimicking the Morphology of Liver Lobule Tissue. *Lab Chip* **2013**, *13*, 3578−3587.
(19) Chen, T.-H.; Zhu, X.; Pan, L.; Zeng, X.; Garfinkel, A.; Tintut, Y.; Demer, L. L.; Zhao, X.; Ho, C.-M. Directing Tissue Morphogenesis via Self-assembly of Vascular Mesenchymal Cells. *Biomaterials* **2012**, *33*, 9019−9026.
(20) Falconnet, D.; Csucs, G.; Grandin, H. M.; Textor, M. Surface Engineering Approaches to Micropattern Surfaces for Cell-based Assays. *Biomaterials* **2006**, *27*, 3044−3063.
(21) Li, N.; Ho, C.-M. Photolithographic Patterning of Organosilane Monolayer for Generating Large Area Two-dimensional B Lymphocyte Arrays. *Lab Chip* **2008**, *8*, 2105−2112.
(22) Ballerini, D. R.; Li, X.; Shen, W. Patterned Paper and Alternative Materials as Substrates for Low-cost Microfluidic Diagnostics. *Microfluid. Nanofluid.* **2012**, *13*, 769−787.
(23) Popova, A. A.; Schillo, S. M.; Demir, K.; Ueda, E.; Nesterov-Mueller, A.; Levkin, P. A. Droplet-array (DA) Sandwich Chip: A Versatile Platform for High-throughput Cell Screening Based on Superhydrophobic-superhydrophilic Micropatterning. *Adv. Mater.* **2015**, *27*, 5217−5222.
(24) Tee, Y. H.; Shemesh, T.; Thiagarajan, V.; Hariadi, R. F.; Anderson, K. L.; Page, C.; Volkmann, N.; Hanein, D.; Sivaramakrishnan, S.; Kozlov, M. M.; Bershadsky, A. D. Cellular Chirality Arising from the Self-organization of the Actin Cytoskeleton. *Nat. Cell Biol.* **2015**, *17*, 445−457.
(25) Zhou, X.; Hu, J.; Li, J.; Shi, J.; Chen, Y. Patterning of Two-Level Topographic Cues for Observation of Competitive Guidance of Cell Alignment. *ACS Appl. Mater. Interfaces* **2012**, *4*, 3888−3892.
(26) Slater, J. H.; Boyce, P. J.; Jancaitis, M. P.; Gaubert, H. E.; Chang, A. L.; Markey, M. K.; Frey, W. Modulation of Endothelial Cell Migration via Manipulation of Adhesion Site Growth Using Nanopatterned Surfaces. *ACS Appl. Mater. Interfaces* **2015**, *7*, 4390−4400.
(27) Doxzen, K.; Vedula, S. R. K.; Leong, M. C.; Hirata, H.; Gov, N. S.; Kabla, A. J.; Ladoux, B.; Lim, C. T. Guidance of Collective Cell Migration by Substrate Geometry. *Integr. Biol.* **2013**, *5*, 1026−1035.
(28) Thakar, R. G.; Cheng, Q.; Patel, S.; Chu, J.; Nasir, M.; Liepmann, D.; Komvopoulos, K.; Li, S. Cell-shape Regulation of Smooth Muscle Cell Proliferation. *Biophys. J.* **2009**, *96*, 3423−3432.
(29) Tang, J.; Peng, R.; Ding, J. The Regulation of Stem Cell Differentiation by Cell-cell Contact on Micropatterned Material Surfaces. *Biomaterials* **2010**, *31*, 2470−2476.
(30) Huo, B.; Lu, X. L.; Guo, X. E. Intercellular Calcium Wave Propagation in Linear and Circuit-like Bone Cell Networks. *Philos. Trans. R. Soc., A* **2010**, *368*, 617−633.
(31) Huo, B.; Lu, X. L.; Costa, K. D.; Xu, Q.; Guo, X. E. An ATP-dependent Mechanism Mediates Intercellular Calcium Signaling in Bone Cell Network under Single Cell Nanoindentation. *Cell Calcium* **2010**, *47*, 234−241.

DOI: 10.1021/acsami.7b15759
ACS Appl. Mater. Interfaces 2018, 10, 2937−2945

(32) Salick, M. R.; Napiwocki, B. N.; Sha, J.; Knight, G. T.; Chindhy, S. A.; Kamp, T. J.; Ashton, R. S.; Crone, W. C. Micropattern Width Dependent Sarcomere Development in Human ESC-derived Cardiomyocytes. *Biomaterials* **2014**, *35*, 4454−4464.
(33) Junkin, M.; Lu, Y.; Long, J.; Deymier, P. A.; Hoying, J. B.; Wong, P. K. Mechanically Induced Intercellular Calcium Communication in Confined Endothelial Structures. *Biomaterials* **2013**, *34*, 2049−2056.
(34) Yuan, Y.; Zha, H.; Rangarajan, P.; Ling, E.-A.; Wu, C. Anti-inflammatory Effects of Edaravone and Scutellarin in Activated Microglia in Experimentally Induced Ischemia Injury in Rats and in BV-2 Microglia. *BMC Neurosci.* **2014**, *15*, 125.
(35) Cao, Q.; Lu, J.; Kaur, C.; Sivakumar, V.; Li, F.; Cheah, P. S.; Dheen, S. T.; Ling, E.-A. Expression of Notch-1 Receptor and Its Ligands Jagged-1 and Delta-1 in Amoeboid Microglia in Postnatal Rat Brain and Murine BV-2 Cells. *Glia* **2008**, *56*, 1224−1237.
(36) Jiang, S. X.; Benson, C. L.; Zaharia, L. I.; Abrams, S. R.; Hou, S. T. Abscisic Acid does not Evoke Calcium Influx in Murine Primary Microglia and Immortalised Murine Microglial BV-2 and N9 Cells. *Biochem. Biophys. Res. Commun.* **2010**, *401*, 435−439.
(37) Shin, S. M.; Cho, K. S.; Choi, M. S.; Lee, S. H.; Han, S.-H.; Kang, Y.-S.; Kim, H. J.; Cheong, J. H.; Shin, C. Y.; Ko, K. H. Urokinase-type Plasminogen Activator Induces BV-2 Microglial Cell Migration through Activation of Matrix Metalloproteinase-9. *Neurochem. Res.* **2010**, *35*, 976−985.
(38) Jiang, P.; Xing, F.; Guo, B.; Yang, J.; Li, Z.; Wei, W.; Hu, F.; Lee, I.; Zhang, X.; Pan, L.; Xu, J. Nucleotide Transmitters ATP and ADP Mediate Intercellular Calcium Wave Communication via $P2Y_{12/13}$ Receptors among BV-2 Microglia. *PLoS One* **2017**, *12*, No. e0183114.
(39) Arcuino, G.; Lin, J. H.-C.; Takano, T.; Liu, C.; Jiang, L.; Gao, Q.; Kang, J.; Nedergaard, M. Intercellular Calcium Signaling Mediated by Point-source Burst Release of ATP. *Proc. Natl. Acad. Sci. U.S.A.* **2002**, *99*, 9840−9845.
(40) Schipke, C. G.; Boucsein, C.; Ohlemeyer, C.; Kirchhoff, F.; Kettenmann, H. Astrocyte Ca^{2+} Waves Trigger Responses in Microglial Cells in Brain Slices. *FASEB J.* **2002**, *16*, 255−257.
(41) Verderio, C.; Matteoli, M. ATP Mediates Calcium Signaling between Astrocytes and Microglial Cells: Modulation by IFN-γ. *J. Immunol.* **2001**, *166*, 6383−6391.
(42) Zhao, H.-B.; Yu, N.; Fleming, C. R. Gap Junctional Hemichannel-mediated ATP Release and Hearing Controls in the Inner Ear. *Proc. Natl. Acad. Sci. U.S.A.* **2005**, *102*, 18724−18729.
(43) Suadicani, S. O.; Brosnan, C. F.; Scemes, E. $P2X_7$ Receptors Mediate ATP Release and Amplification of Astrocytic Intercellular Ca^{2+} Signaling. *J. Neurosci.* **2006**, *26*, 1378−1385.
(44) Bowser, D. N.; Khakh, B. S. Vesicular ATP is the Predominant Cause of Intercellular Calcium Waves in Astrocytes. *J. Gen. Physiol.* **2007**, *129*, 485−491.
(45) Anderson, C. M.; Bergher, J. P.; Swanson, R. A. ATP-induced ATP Release from Astrocytes. *J. Neurochem.* **2004**, *88*, 246−256.
(46) Hassinger, T. D.; Guthrie, P. B.; Atkinson, P. B.; Bennett, M. V. L.; Kater, S. B. An Extracellular Signaling Component in Propagation of Astrocytic Calcium Waves. *Proc. Natl. Acad. Sci. U.S.A.* **1996**, *93*, 13268−13273.
(47) MacDonald, C. L.; Yu, D.; Buibas, M.; Silva, G. A. Diffusion Modeling of ATP Signaling Suggests a Partially Regenerative Mechanism Underlies Astrocyte Intercellular Calcium Waves. *Front. Neuroeng.* **2008**, *1*, 1−13.
(48) Warren, N. J.; Tawhai, M. H.; Crampin, E. J. Mathematical Modelling of Calcium Wave Propagation in Mammalian Airway Epithelium: Evidence for Regenerative ATP release. *Exp. Physiol.* **2010**, *95*, 232−249.
(49) Jiang, X.; Bruzewicz, D. A.; Wong, A. P.; Piel, M.; Whitesides, G. M. Directing Cell Migration with Asymmetric Micropatterns. *Proc. Natl. Acad. Sci. U.S.A.* **2005**, *102*, 975−978.
(50) Brock, A.; Chang, E.; Ho, C.-C.; LeDuc, P.; Jiang, X.; Whitesides, G. M.; Ingber, D. E. Geometric Determinants of Directional Cell Motility Revealed Using Microcontact printing. *Langmuir* **2003**, *19*, 1611−1617.
(51) Small, J. V.; Stradal, T.; Vignal, E.; Rottner, K. The Lamellipodium: Where Motility Begins. *Trends Cell Biol.* **2002**, *12*, 112−120.
(52) Clark, A. J.; Petty, H. R. Observation of Calcium Microdomains at the Uropod of Living Morphologically Polarized Human Neutrophils Using Flash Lamp-based Fluorescence Microscopy. *Cytometry, Part A* **2008**, *73*, 673−678.
(53) Tsai, F.-C.; Meyer, T. Ca^{2+} Pulses Control Local Cycles of Lamellipodia Retraction and Adhesion along the Front of Migrating Cells. *Curr. Biol.* **2012**, *22*, 837−842.
(54) Tsai, F.-C.; Seki, A.; Yang, H. W.; Hayer, A.; Carrasco, S.; Malmersjö, S.; Meyer, T. A Polarized Ca^{2+}, Diacylglycerol and STIM1 Signalling System Regulates Directed Cell Migration. *Nat. Cell Biol.* **2014**, *16*, 133−144.
(55) Wei, C.; Wang, X.; Chen, M.; Ouyang, K.; Song, L.-S.; Cheng, H. Calcium Flickers Steer Cell Migration. *Nature* **2009**, *457*, 901−905.
(56) Visser, D.; Langeslag, M.; Kedziora, K. M.; Klarenbeek, J.; Kamermans, A.; Horgen, F. D.; Fleig, A.; van Leeuwen, F. N.; Jalink, K. TRPM7 Triggers Ca^{2+} Sparks and Invadosome formation in Neuroblastoma Cells. *Cell Calcium* **2013**, *54*, 404−415.

DOI: 10.1021/acsami.7b15759
ACS Appl. Mater. Interfaces 2018, 10, 2937−2945